AGU PUBLICATIONS

JGR

Journal of Geophysical Research: Biogeosciences

RESEARCH ARTICLE

10.1002/2013JG002502

Key Points:
- CG flash rate is simulated to increase by up to 21% at the end of the century
- Global burned area was little affected by these changes
- However, there were considerable changes on the regional scale

Correspondence to:
A. Krause,
andreas.krause@zmaw.de

Citation:
Krause, A., S. Kloster, S. Wilkenskjeld, and H. Paeth (2014), The sensitivity of global wildfires to simulated past, present, and future lightning frequency, *J. Geophys. Res. Biogeosci.*, *119*, 312–322, doi:10.1002/2013JG002502.

Received 21 SEP 2013
Accepted 9 FEB 2014
Accepted article online 14 FEB 2014
Published online 20 MAR 2014

The sensitivity of global wildfires to simulated past, present, and future lightning frequency

Andreas Krause[1,2,3], Silvia Kloster[2], Stiig Wilkenskjeld[2], and Heiko Paeth[1]

[1]Institute of Geography and Geology, University of Würzburg, Würzburg, Germany, [2]Land in the Earth System, Max Planck Institute for Meteorology, Hamburg, Germany, [3]Now at Institute for Meteorology and Climate Research - Atmospheric Environmental Research, Karlsruhe Institute of Technology, Garmisch-Partenkirchen, Germany

Abstract In this study, components of the Max Planck Institute Earth System Model were used to explore how changes in lightning induced by climate change alter wildfire activity. To investigate how climate change alters global flash frequency, simulations with the atmospheric general circulation model ECHAM6 were performed for the time periods preindustrial, present-day, and three future scenarios. The effect of changes in lightning activity on fire occurrence was derived from simulations with the land surface vegetation model JSBACH. Global cloud-to-ground lightning activity decreased by 3.3% under preindustrial climate and increased by up to 21.3% for the RCP85 projection at the end of the century when compared to present-day, respectively. Relative changes were most pronounced in North America and northeastern Asia. Global burned area was little affected by these changes and only increased by up to 3.3% for RCP85. However, on the regional scale, significant changes occurred. For instance, burned area increases of over 100% were found in high-latitude regions, while also several regions were identified where burned area declined, such as parts of South America and Africa.

1. Introduction

Wildfires are frequent events on Earth occurring in almost all vegetation-covered locations. At present 330–431 Mha of the Earth's vegetation burn annually [*Giglio et al.*, 2010], resulting in a release of 2–4 Pg C to the atmosphere [*Bowman et al.*, 2009]. Fires are driven by climate and weather conditions and depend on fuel load availability. On the other hand, fires alter vegetation composition and abundance and thereby also affect surface properties, biochemical cycles, and atmospheric chemistry [*Thonicke et al.*, 2001; *Bowman et al.*, 2009; *Ward et al.*, 2012].

During the last decades, several modeling studies using different approaches have explored the impact of climate change on regional or global fire activity [see *Flannigan et al.*, 2009]. However, most of these studies focused on changes in temperature and precipitation, keeping other important factors like ignition agents constant.

Lightning strokes are the most important natural ignition source for wildfires. While presently, the majority of worldwide fires are started intentionally or accidentally by humans, lightning ignitions predominate in several regions like the boreal zone where a small number of fires are usually responsible for most of the total burned area [*Stocks et al.*, 2002].

Global flash rate is expected to respond to climate change as it is correlated with temperature on short time scales [*Williams*, 2005]. However, due to limited observational data and a lack of understanding of lightning physics, it is not assured if and to what extent this connection also holds on the time scale of climate change [*Dwyer and Rassoul*, 2009; *Price*, 2009]. Modeling studies exploring the behavior of global lightning activity in the future with a general circulation model (GCM) generally use parameterizations which utilize the relationship between flash rates and other meteorological variables like convective cloud top height, precipitation, or convective mass flux [e.g., *Price and Rind*, 1992; *Allen and Pickering*, 2002]. These studies predict an increase in lightning activity with warming of roughly 5–10% for every degree warming [e.g., *Price and Rind*, 1994a; *Michalon et al.*, 1999]. Only few studies examined the implications on fire activity. *Price and Rind* [1994b] and *Goldammer and Price* [1998] used the GISS climate model for regional applications. *Price and Rind* [1994b] found an increase in burned area of 78% for the United States in a $2XCO_2$ world and both

studies assumed substantial increases in lightning-caused fires in the tropics, however, without providing any quantification.

In this study we used components of the Earth System Model of the Max Planck Institute for Meteorology (MPI-ESM) [*Giorgetta et al.*, 2013] to simulate the impact of climate-change induced changes in lightning activity on fire occurrence globally for different climate states. The main research questions in our study were how climate change alters lightning activity and how this, in turn, will impact fire occurrence. While global fire modeling has made some progress over the last years, thanks to satellite observations on fire activity that help to constrain those models, only a limited number of studies investigated how fire occurrence will change with changing climate [*Flannigan et al.*, 2009]. To our knowledge only two studies explicitly took into account the impact of the changing climate on lightning activity and subsequent changes in future fire occurrence [*Price and Rind*, 1994b; *Goldammer and Price*, 1998], which were, however, limited due to very coarse model resolution and their assumptions on future climate change projections. To close this gap, we implemented a lightning parameterization into the atmospheric component of the MPI-ESM (ECHAM6) [*Stevens et al.*, 2013] and performed simulations for a range of climate conditions: near past, present, and future, with climate projections in accordance with the recent Coupled Model Intercomparison Project (CMIP5) [*Taylor et al.*, 2012]. Then we forced the vegetation model of the MPI-ESM (JSBACH) [*Raddatz et al.*, 2007; *Reick et al.*, 2013] with the resulting flash rates and analyzed the simulated burned area. To our knowledge this is the first study that uses a state of the art ESM to estimate the sensitivity of global burned area to climate-induced changes in lightning activity. The paper is structured as follows: While sections 2 and 3 provide information about the model and the simulation setup, the results are presented and discussed in section 4. Section 5 contains the conclusions of this work.

2. Model Description

All experiments were performed with components of the MPI-ESM. The lightning simulations were performed with the atmospheric GCM ECHAM6 and burned area was simulated in the land surface vegetation model JSBACH with an implemented fire model [*Arora and Boer*, 2005; *Kloster et al.*, 2010].

Lightning in ECHAM6 was calculated using the global lightning parameterization of *Price and Rind* [1992] which has been used in numerous modeling studies [e.g., *Michalon et al.*, 1999]. This approach takes advantage of the nonlinear correlation between continental flash rates F_c (flashes/min/gridbox) and convective cloud top height H (km) given by

$$F_c = C \cdot 3.44 \cdot 10^{-5} H^{4.90} \tag{1}$$

As maritime thunderstorms produce less lightning than thunderstorms over land with similar cloud top heights, *Price and Rind* [1992] suggested a separate equation over the oceans

$$F_m = C \cdot 6.40 \cdot 10^{-4} H^{1.73} \tag{2}$$

where F_m is the maritime flash frequency of the grid box and C is a resolution- and model-dependent scaling factor which was set to 0.107 to reproduce global climatological mean flash rates observed from satellites ($\sim$ 46 flashes/s, see section 4 of this paper).

Convection in ECHAM6 is parameterized by the scheme of *Tiedtke* [1989] with an extension for deep convection designed by *Nordeng* [1994]. How sensitive the *Price and Rind* [1992] parameterization is to the convection scheme has been shown by *Tost et al.* [2007]. The authors concluded that the cloud top height approach is quite robust to both spatial and temporal variations of the convective events. Wildfires can only be ignited when the lightning stroke reaches the ground, making it necessary to explicitly calculate the ratio z of intracloud (IC) to cloud-to-ground (CG) lightning. *Price and Rind* [1993] suggested to derive z from the cold cloud depth ΔH (km), which is defined from the 0° layer above cloud base to the cloud top, by

$$z = 0.021(\Delta H)^4 - 0.648(\Delta H)^3 + 7.493(\Delta H)^2 - 36.54(\Delta H) + 63.09 \tag{3}$$

This is due to the fact that as the cold cloud sector expands, the electric field gets stronger, which favors immediate electric breakdown and thereby IC lightning.

Table 1. Simulation Setup for the Lightning Experiments: Name of the Experiment, Corresponding Time Period, Average Global Warming, Total and CG Flash Frequency, and Relative Differences Compared to the PD Simulation

Experiment	Forcing[a]	ΔT(°C)[b]	Total Flashes/s	Diff. to PD (%)	CG Flashes/s	Diff. to PD (%)
PI	1850–1874	−1.17	44.20 ± 1.46	−4.84	6.13 ± 0.18	−3.31
PD	1980–2004	0.0	46.45 ± 0.87	0	6.34 ± 0.12	0
RCP26	2070–2094	0.40	48.65 ± 1.35	+4.74	6.52 ± 0.16	+2.84
RCP45	2070–2094	1.27	52.53 ± 2.21	+13.09	6.82 ± 0.25	+7.57
RCP85	2070–2094	2.83	60.91 ± 2.25	+31.13	7.69 ± 0.21	+21.29

[a]SSTs and SIC from the MPI-ESM CMIP5 experiments [*Giorgetta et al.*, 2013] were prescribed in ECHAM6.
[b]Difference to PD.

Vegetation fires were computed using the *Arora and Boer* [2005] fire algorithm, which was for this study implemented into JSBACH. This algorithm calculates the total fire occurrence probability (P_f) as the product of three functions representing the availability of biomass (P_b), fuel moisture (P_m), and ignition source (I). P_b is constrained by the aboveground biomass simulated in JSBACH and scales linearly between a minimum (200 g C/m^2) and maximum (1000 g C/m^2) biomass. P_m depends on soil moisture which is used as a surrogate for fuel moisture that is not explicitly calculated in JSBACH. P_m reaches the value 0 once the soil moisture exceeds the extinction wetness content (0.35). The area burned is assumed to form an elliptical shape around the point of ignition defined by the fire spread rate in downwind direction and the length-to-breadth ratio of the ellipse. The fire spread rate in downwind direction is parameterized as a sigmoidal function of wind speed and soil moisture, which plateaus at the maximum spread rate. With higher wind speeds and drier conditions, the fire spreads faster. The length-to-breadth ration of the ellipse is a function of wind speed (with higher wind speeds, a more elongated shape is assumed). The *Arora and Boer* [2005] fire algorithm was implemented into JSBACH similar to its implementation into the vegetation model CLM-CN [*Kloster et al.*, 2010] with further updates from *Li et al.* [2012]. Instead of a probability function, the *Li et al.* [2012] update is based on the number of ignitions that can start a fire (I)

$$I = \text{eff} \cdot CG \tag{4}$$

CG denotes CG flashes (flashes/timestep/gridbox) and the eff factor scales the total number of CG flashes to those that actually carry enough energy to ignite a fire. We set eff to 0.001 following *Hall* [2007]. In addition to that, the average maximum fire spread rate was made a plant functional type dependent parameter, the head-to-back ratio of the burned ellipse was calculated as a function of the length-to-breadth ratio, and the parameter $g(0)$ used to calculate the fire spread rate in downwind direction was changed from 0.1 to 0.05 as suggested by *Li et al.* [2012]. We did not account for anthropogenic ignitions and fire suppression in this study.

3. Simulation Setup

To investigate the influence of climate change on global lightning activity we performed five simulations with ECHAM6. These simulations were performed with prescribed sea surface temperatures (SSTs) and sea ice cover (SIC) for different climate states. SSTs and SIC were extracted from fully coupled MPI-ESM simulations conducted for CMIP5. We used the following forcing climates: pre-industrial (PI, for the time period 1850–1874), present-day (PD, 1980–2004), and three different Representative Concentration Pathways (RCP26, RCP45, and RCP85, in each case 2070–2094) projections (Table 1). The RCP's number expresses its radiative forcing level in 2100, e.g., the RCP26 projection leads to a radiative forcing of 2.6 W m^{-2} at the end of this century [*Moss et al.*, 2010]. We chose a time interval of 25 years as a compromise between the need of sufficiently long runs for climate analyses and limited computing time. We applied ECHAM6 in T63 (~1.875° × 1.875°) resolution with 47 vertical layers in the atmosphere up to 10 hPa (CMIP5-low resolution (LR) setup) for which atmospheric greenhouse gas concentrations were prescribed according to the CMIP5 protocol.

The fire experiments were performed by the land carbon submodel (CBALANCE) of JSBACH. The CBALANCE model describes the changes in carbon storage from the growth and death of plants and the remineralization of carbon in soils including natural disturbances such as fires and windbreak. CBALANCE is forced

Table 2. Total Global Burned Area and Relative Changes Compared to PD for the Different Fire Simulations

Experiment	Forcing Climate[a]	Forcing Lightning	Annual Burned Area (Mha)	Diff. to PI_PD (%)
PI_PI	PI	PI	586.2 ± 30.9	−0.2
PI_PD	PI	PD	587.6 ± 41.0	0
PI_RCP26	PI	RCP26	578.5 ± 50.4	−1.6
PI_RCP45	PI	RCP45	591.0 ± 44.9	+0.6
PI_RCP85	PI	RCP85	606.8 ± 39.5	+3.3
RCP85_PD	RCP85	PD	848.6 ± 77.2	+44.4
RCP85_RCP85	RCP85	RCP85	875.7 ± 74.3	+49.0

[a]Forcing data from the MPI-ESM CMIP5 experiments were extracted to drive the carbon submodel of the land surface vegetation model JSBACH.

with net primary productivity, leaf area index, and climate variables (soil moisture, relative humidity, temperature, and wind). The forcing variables were extracted from the CMIP5 simulations performed with the MPI-ESM [*Giorgetta et al.*, 2013] during the time slices mentioned above. In total, we performed seven fire experiments. In each experiment, vegetation distribution was kept at the 1850 settings. While we used the same forcing climate in each of the first five simulations (PI climate, daily values), we prescribed the flash rates as averaged monthly CG lightning frequency from the previously described lightning experiments in order to be able to estimate the "lightning impact" caused by a changing climate without the direct climate effects (see Table 2). We refer to these simulations as PI_PI, PI_PD, PI_RCP26, PI_RCP45, and PI_RCP85. We used a repeating 25 year climate and lightning cycle for each experiment until the carbon pools were in an equilibrium state which was reached after 400 years (except for the slow carbon pool which does not interact with the fire variables analyzed here). The equilibrium state was defined as the state with near zero changes in the carbon pool sizes when averaged over the 25 year cycling period. The last cycle was used for the analyses.

We were also interested in the changes in burned area caused by the direct climate impact on fuel load and state only. In addition, we analyzed the impact of only lightning changes on burned area in a different climate. Therefore, we performed two additional experiments: In one, in the following referred to as RCP85_RCP85, besides lightning frequency, we also used the forcing climate from the CMIP5 RCP85 simulation, thereby affecting fire activity by both changes in flash frequency and climate conditions (see Table 2). We chose RCP85 climate exemplary as it features the most extreme climate change of the scenarios we used. In a second experiment, RCP85_PD, we used the RCP85 climate again but now with PD lightning activity.

4. Results and Discussion

The first part of this section contains the results from the lightning simulations and a comparison of the PD experiment with observed lightning activity. In the second part of the chapter the fire simulations will be analyzed.

4.1. Lightning Results

Figure 1 shows the annual total lightning pattern as simulated in the PD experiment. It is compared to the Lightning Imaging Sensor (LIS)/Optical Transient Detector (OTD) climatology data set made available by NASA (http://thunder.nsstc.nasa.gov, last accessed August 2013). These data sets consist of gridded total lightning flashes (IC and CG lightning) as seen by the space-borne LIS (1997 to present) [*Christian et al.*, 1999] and the OTD (1995–2000) [*Boccippio et al.*, 2000]. The data set used in this study is the High-Resolution Monthly Climatology [see *Cecil et al.*, 2014]. The general pattern is quite coherent between model and observations: Most lightning occurs over the tropical land areas while lightning is rare over the oceans. ECHAM6 tends to underestimate lightning activity over central Africa, in midlatitudes and over the oceans. On the other hand, the model overestimates flash rates over equatorial South America, Southeastern Asia, and Northern Australia. The Pearson correlation coefficient between modeled and observed flash rates is 0.69 over the continents. While modeled flash rates in 16% of the land area where lightning occurs differ by less than 20% from observations, 58% of the continental areas produce differences of more than 50%, mostly in regions of low flash rates. The model satisfactorily reproduces the seasonal cycle, and the month of peak lightning activity is for most regions in agreement with the LIS/OTD climatology. Exceptions are regions in the deep tropics in South America and parts of South Asia (Figure 2).

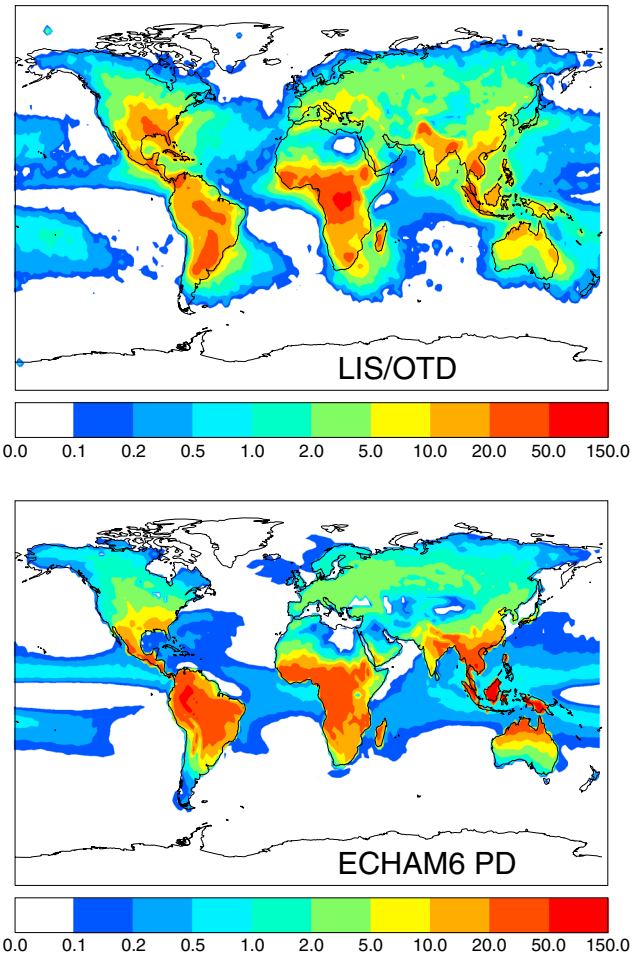

Figure 1. Annual total lightning flash frequency for (top) LIS/OTD (1995–2010) and (bottom) ECHAM6 PD (1980–2004) in flashes/km^2/year. Note that the scale used here is nonlinear.

Total average annual global lightning activity for each simulation is presented in Table 1. While average PI global lightning activity is about 5% lower than PD, RCP26, RCP45, and RCP85 produce 5, 13, and 31% more flashes, respectively. Contrary to *Price and Rind* [1994a], CG frequency increases less than total lightning due to smaller increases in freezing level height compared to cloud top height resulting in a considerable reduction in CG/total lightning ratio particularly over land areas as seen in Figure 3). The Figure shows the spatial distribution of CG lightning percentage for PD and RCP85 and differences between those scenarios. In both cases, the CG/total lightning ratio peaks in high latitudes over the continents. In the tropics, the proportion of CG lightning is smaller than the approximately 22% reported in *Price and Rind* [1994c], but in agreement with ground observations by *Pinto et al.* [2007] who, on the other hand, reported similar CG/total lightning ratios in temperate regions. Virtually all land regions are affected by decreases in CG percentage in RCP85; however, the number of CG flashes usually still increase due to increased total flash frequencies.

Looking at the spatial distribution of CG lightning for the different experiments (Figure 4) reveals that despite increasing temperatures (Table 1), CG flash frequency decreases over much of the oceans and over parts of Europe, India, West Africa, and,

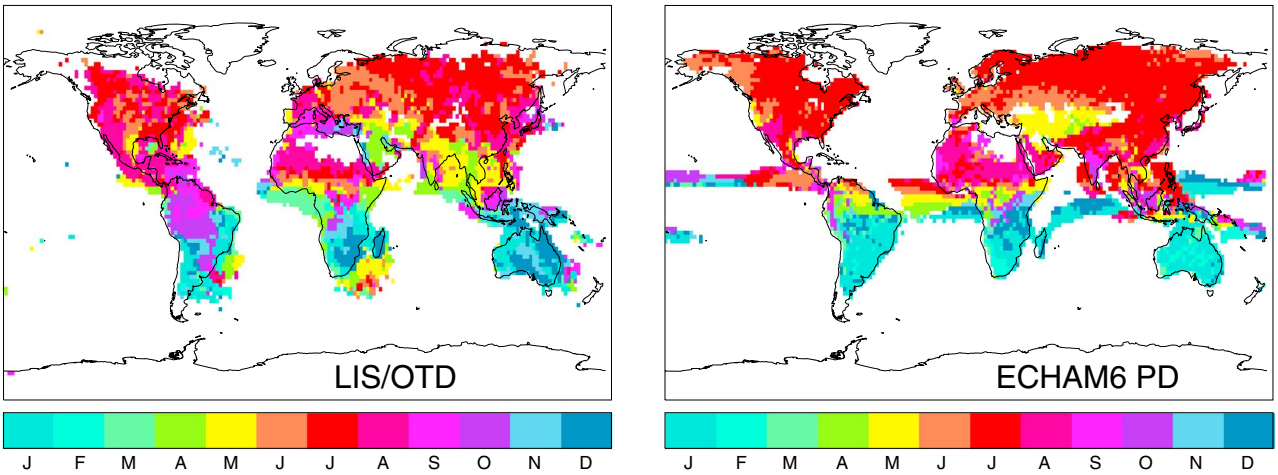

Figure 2. Calendar month of maximum lightning activity for (left) LIS/OTD and (right) ECHAM6. Only regions where peak monthly lightning activity exceeds 0.01 flashes/km^2 are shown.

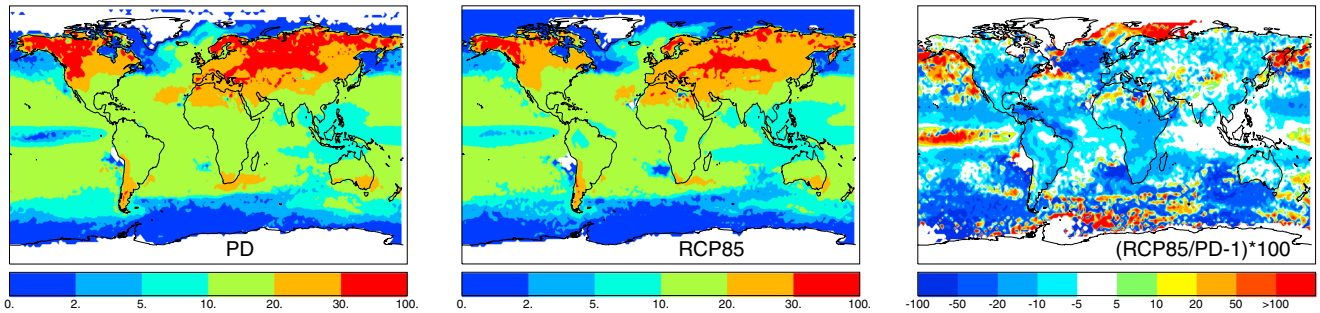

Figure 3. Cloud-to-ground percentage of total lightning for (left) PD, (middle) RCP85, and (right) the relative difference between both.

particularly, over northeastern South America. Other continental regions generally produce more CG lightning in a warmer world. Absolute changes are greatest in the tropics, while relative changes are most pronounced in North America and northeastern Asia. Interestingly, CG lightning over Australia is much less for PI, RCP26, and RCP45 compared to the PD simulation, while RCP85 produces more lightning. This

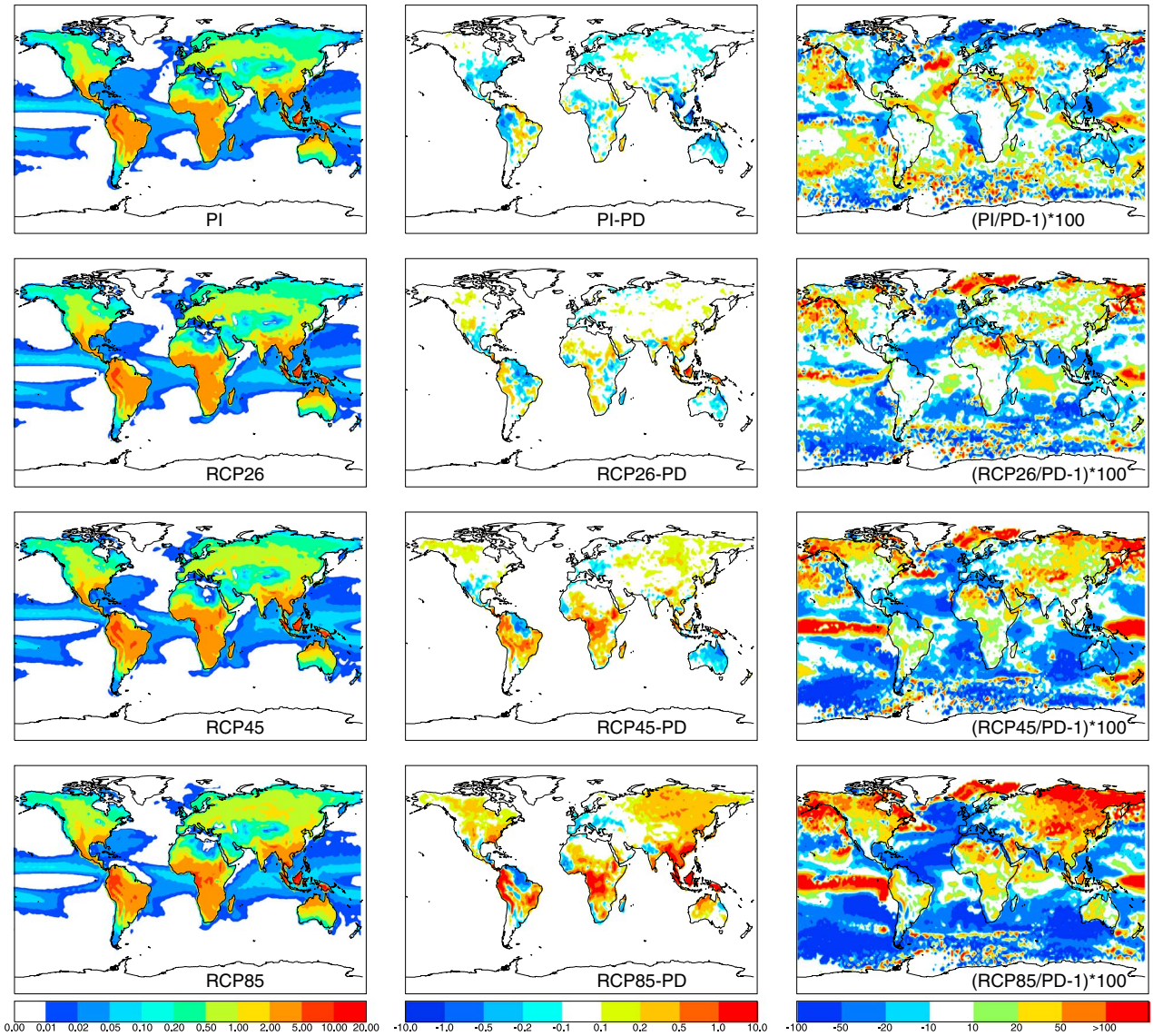

Figure 4. Annual cloud-to-ground lightning flash frequency in (left) flashes/km^2/year, (middle) absolute difference compared to PD, and (right) relative change for PI, RCP26, RCP45, and RCP85 (from top to the bottom).

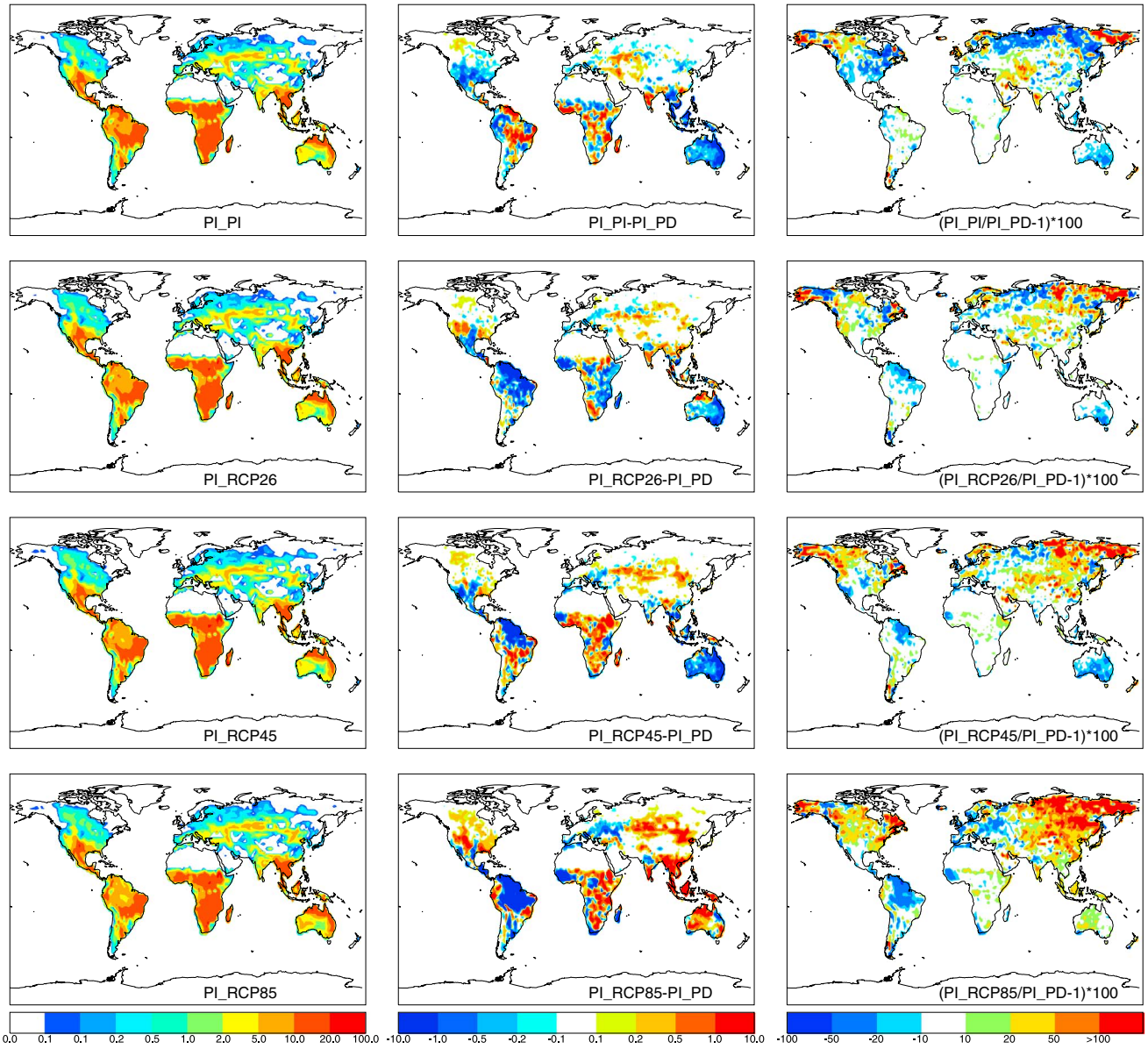

Figure 5. (left) Annual burned fraction, (middle) absolute difference compared to PI_PD, and (right) relative change for PI_PI, PI_RCP26, PI_RCP45, and PI_RCP85 (from top to the bottom).

might be caused by the nonlinear relationship between lightning response or CG ratio to changes in cloud top height or cold cloud depth (equations (1) and (3)), that in turn are nonlinear related to changes in climate. Why particularly the RCP85 scenario with the strongest global warming leads to reversed changes in lightning activity compared to the other projections over Australia cannot be directly derived from our simulation data, but is an interesting feature for future studies.

4.2. Fire Results

Average global fire activity, despite significant annual variations, is quite similar amongst the experiments forced by PI climate and different lightning activity and reaches values between 578 ± 50 (PI_RCP26) and 607 ± 39 (PI_RCP85) Mha/yr (see Table 2). These values are greater than fire activity estimated from satellite measurements (330–431 Mha/yr) [*Giglio et al.*, 2010]. However, the simulations presented here do not account for human-fire interactions (ignition and suppression) and the prescribed potential vegetation cover is representative for pre-industrial times. As such, the simulations are not directly comparable to present-day satellite-based observations. However, burned area for pre-industrial land coverage is expected

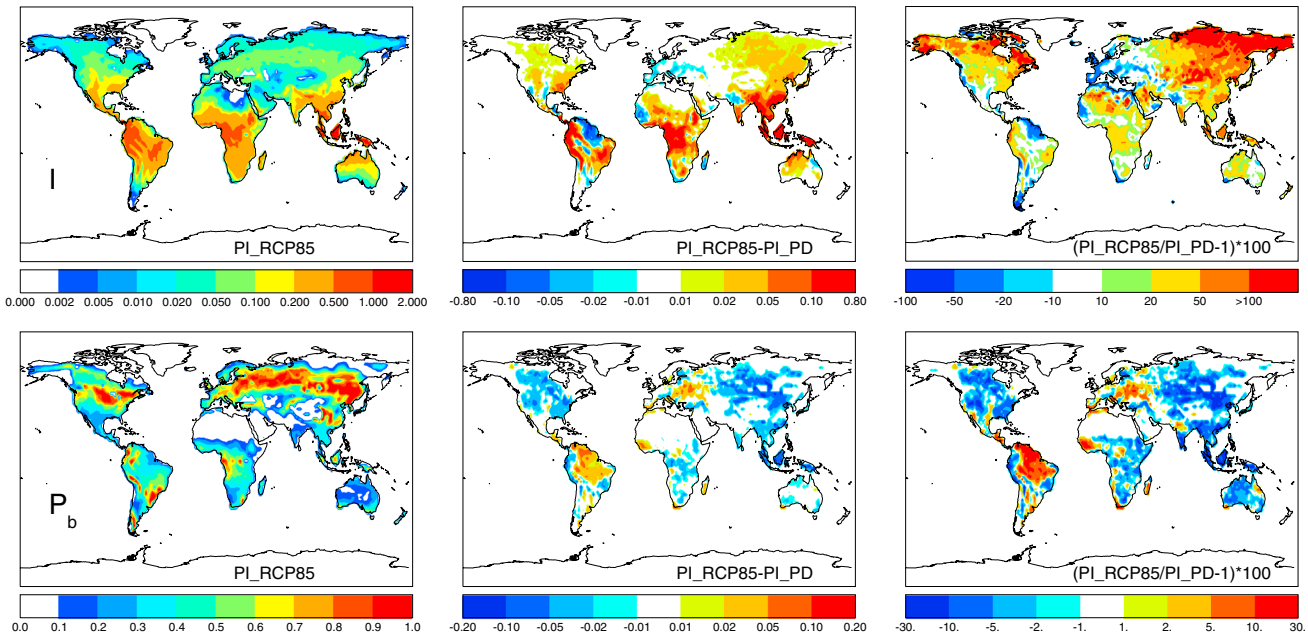

Figure 6. Averaged ignition probability for (left) PI_RCP85,(middle) absolute difference compared to PI_PD, and (right) relative change for (top) ignition sources I and (bottom) biomass availability P_b. Note that the scales are different.

to be higher than present-day burning as less land area was anthropogenically managed [*Marlon et al.*, 2008; *Kloster et al.*, 2012; *van der Werf et al.*, 2013]. Similar to satellite estimates [*Giglio et al.*, 2010], most fires occur in sub-Saharan Africa, southeastern Asia, northern Australia, and parts of North and South America, while there is little fire activity in high latitudes and in the deserts of the world (Figure 5). The model, however, likely overestimates burned area in equatorial South America, southern North America, central Africa, and southeastern Asia.

Changes in fire activity mostly match CG flash rate changes (compare Figures 4 and 5). For example, fire activity for PI_RCP85 increases in most parts of Africa (+2.79%), Australia (+7.42%), continental Asia (+18.03%), North America (+10.77%), and particularly Southeast Asia (+32.88%), while it decreases in Europe (−10.80%) and South America (−10.71%). Especially in Eastern Canada and Siberia, regions that nowadays are characterized by low flash rates, lightning changes seem to be important and result in relative increases in burned area of often more than 100%. These changes can usually be explained by changes in ignition sources I (Figure 6). However, burned area is not only controlled by changes in lightning activity but also through changes in fuel load availability induced by changes in fire activity itself. Thus, biomass probability, expressed as P_b, generally decreases in areas where flash rate increases and vice versa (Figure 6).

While climate change influences burned area through changes in lightning activity, it will also impact burned area through changes in fuel availability and fuel moisture, which are in turn controlled by, e.g., temperature and precipitation. These direct global warming effects lead, in case of the RCP85 climate (RCP85_PD), to a 44.4% increase in burned area (see Table 2), partly due to strong increases in available fuel load, and are thus much stronger than the lightning impact. When forcing climate and lightning activity are both taken from RCP85 (RCP85_RCP85), burned area is about 49.0% higher than under PD conditions.

Interestingly, while the difference in global burned area between RCP85_RCP85 and RCP85_PD is quite similar to the difference between PI_RCP85 and PI_PD on the global scale (4.6% compared to 3.3%, see Table 2), on the regional scale the climate state is important in many regions. This implies that the lightning impact on burned area depends on the prescribed climate state. The differences between the absolute values of the change in burned area caused by lightning changes in the two different climate states are presented in Figure 7. The impact of the climate state is greatest in Asia and North America where the differences between the two climate states are often more than 50% (in both directions) which coincides with the areas in which the relative lightning impact on fire occurrence is strongest. However, the climate state is also important in areas of high fire activity such as South America (where the reduction of burned area is

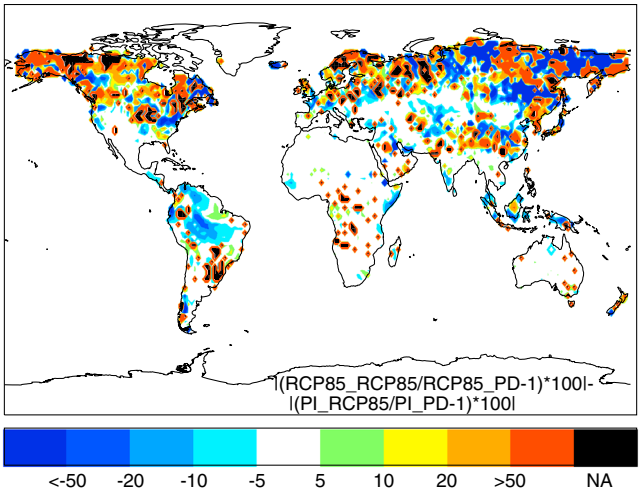

Figure 7. Difference between the absolute values of (RCP85_RCP85/RCP85_PD-1)*100 and (PI_RCP85/PI_PD-1)*100. Changes are greater from PI_PD to PI_RCP85 than from RCP85_PD to RCP85_RCP85 for blue colors and vice versa, which means the impact of the corresponding climate state (PI or RCP85) is more important in the respective region. Black regions indicate regions where the sign of difference is different for the two climate states.

considerably smaller from RCP85_PD to RCP85_RCP85 than from PI_PD to PI_RCP85) or Indonesia (where burned area increases with RCP85 lightning activity). Africa and Australia seem to be hardly affected by the climate state.

5. Conclusions

In this work we used components of the MPI-ESM to investigate the influence of climate change on global lightning activity and associated changes in burned area. We showed that ECHAM6, by using the parameterization of *Price and Rind* [1992], is able to simulate present-day global flash rates reasonably well, which is demonstrated by a correlation coefficient of 0.69 over land. Global annual total and CG lightning activity are projected to increase by 5, 13, and 31% and 3, 8, and 21% for the RCP26, RCP45, and RCP85 scenario, respectively, compared to PD. While absolute increases are greatest in the tropics, relative increases are most pronounced in northern North America and Asia. Flash frequencies over most maritime regions decrease with increasing temperatures. We found considerable changes in fire activity caused by changes in CG lightning frequency in many regions; however, these changes more or less even out on the global scale. The findings of *Price and Rind* [1994b] and *Goldammer and Price* [1998] that lightning-ignited fires will increase mostly in the tropics cannot be confirmed by our results, which show greatest increases in northern latitudes and a decline in many tropical areas. When we changed the forcing climate to RCP85, burned area increased by more than 44% for RCP85_PD and 49% for RCP85_RCP85 due to changes in fuel load, fuel moisture, and, for the latter, flash frequency. Thus, other impacts of climate change that control fire occurrence through changes in fuel availability and moisture on a global scale are significantly stronger than the lightning impact alone. In addition, our simulations also demonstrate that the impact of changing lightning activity on fire occurrence depends on the climate state.

Our results suggest a significant shift in fire patterns in many regions around the globe through a mechanism that was hardly considered in previous climate change studies that assumed that fuel type and fuel state are much more important than lightning ignitions [e.g., *Krawchuk et al.*, 2009; *Fauria et al.*, 2010]. While our study confirms that climate-induced changes in fuel availability and fuel moisture indeed outweigh the impact of changes in lightning ignitions on the global scale, we also show that changes in flash frequency significantly alter fire activity in many regions and should be accounted for in any future modeling studies dealing with burned area.

However, our approach also suffers from several limitations. Lightning and fire are not completely understood, both processes are roughly parameterized in climate models and our ability to forecast lightning and fire in global warming scenarios is currently very limited [e.g., *Dwyer and Rassoul*, 2009; *Price*, 2009; *Fauria et al.*, 2010]. In this study we combined the results of a lightning and a fire model, the uncertainties related to

lightning parameterizations, therefore, propagate into our fire model results. Alternative lightning parameterizations, which do rely on other predictors than the highly nonlinear cloud top height, could potentially produce a different sensitivity to temperature changes. Even if the same lightning and fire parameterization is used, both processes' response to global warming could significantly shift by the use of a different atmospheric or vegetation model or another model resolution [e.g., *Tost et al.*, 2007; *Kloster et al.*, 2012].

Despite these limitations, our results can still be seen as a small but important step toward reliable projections of wildfires in a future climate. For the first time, the impact of changes in flash frequencies on global burned area was estimated by using components of a state of the art ESM. The experiments rely on well-established lightning and fire parameterizations and on recently performed coupled climate simulations (CMIP5), and can therefore not only provide an estimation of future burned area, but can also be a valuable tool for researchers interested in the prediction of changes in global lightning activity itself.

Acknowledgments
We thank Martin Schultz for providing the code of the lightning parameterization. We are also grateful to Anne Dallmeyer and two anonymous reviewers for reviewing the text.

References

Allen, D. J., and K. E. Pickering (2002), Evaluation of lightning flash rate parameterizations for use in a global chemical transport model, *J. Geophys. Res.*, *107*(D23), 4711, doi:10.1029/2002JD002066.

Arora, V. K., and G. J. Boer (2005), Fire as an interactive component of dynamic vegetation models, *J. Geophys. Res.*, *110*, G02008, doi:10.1029/2005JG000042.

Boccippio, D. J., W. Koshak, R. Blakeslee, K. Driscoll, D. Mach, D. Buechler, W. Boeck, H. J. Christian, and S. J. Goodman (2000), The Optical Transient Detector (OTD): Instrument characteristics and cross-sensor validation, *J. Atmos. Oceanic Technol.*, *17*, 441–458, doi:10.1175/1520-0426(2000)017<0441:TOTDOI>2.0.CO;2.

Bowman, D. M., et al. (2009), Fire in the Earth system, *Science*, *324*(5926), 481–484, doi:10.1126/science.1163886.

Cecil, D. J., D. E. Buechler, and R. J. Blakeslee (2014), Gridded lightning climatology from TRMM-LIS and OTD: Dataset description, *Atmos. Res.*, *135–136*, 404–414, doi:10.1016/j.atmosres.2012.06.028.

Christian, H. J., et al. (1999), The lightning imaging sensor, *Proceedings of the 11th International Conference on Atmospheric Electricity*, pp. 746–749, Guntersville, Alabama.

Dwyer, J. R., and H. K. Rassoul (2009), Lightning physics and the study of climate change and sustainability, *AIP Conf. Proc.*, *1157*(26), 26–31, doi:10.1063/1.3208027.

Fauria, M. M., S. T. Michaletz, and E. A. Johnson (2010), Predicting climate change effects on wildfires requires linking processes across scales, *Wiley Interdiscip. Rev. Clim. Change*, *2*(1), 99–112, doi:10.1002/wcc.92.

Flannigan, M. D., M. A. Krawchuk, W. J. de Groot, B. M. Wotton, and L. M. Gowman (2009), Implications of changing climate for global wildland fire, *Int. J. Wildland Fire*, *18*(5), 483–507, doi:10.1071/WF08187.

Giglio, L., J. T. Randerson, G. R. van der Werf, P. S. Kasibhatla, G. J. Collatz, D. C. Morton, and R. S. DeFries (2010), Assessing variability and long-term trends in burned area by merging multiple satellite fire products, *Biogeosciences*, *7*, 1171–1186, doi:10.5194/bg-7-1171-2010.

Giorgetta, M. A., et al. (2013), Climate and carbon cycle changes from 1850 to 2100 in MPI-ESM simulations for the Coupled Model Intercomparison Project phase 5, *J. Adv. Model. Earth Syst.*, *5*, 572–597, doi:10.1002/jame.20038.

Goldammer, J. G., and C. Price (1998), Potential impacts of climate change on fire regimes in the tropics based on MAGICC and a GISS GCM-derived lightning model, *Clim. Change*, *39*, 273–296, doi:10.1023/A:1005371923658.

Hall, B. L. (2007), Precipitation associated with lightning-ignited wildfires in Arizona and New Mexico, *Int. J. Wildland Fire*, *16*(2), 242–254, doi:10.1071/WF06075.

Kloster, S., N. M. Mahowald, J. T. Randerson, P. E. Thornton, F. M. Hoffman, S. Levis, P. J. Lawrence, J. J. Feddema, K. W. Oleson, and D. M. Lawrence (2010), Fire dynamics during the 20th century simulated by the Community Land Model, *Biogeosciences*, *7*, 1877–1902, doi:10.5194/bg-7-1877-2010.

Kloster, S., N. M. Mahowald, J. T. Randerson, and P. J. Lawrence (2012), The impacts of climate, land use, and demography on fires during the 21st century simulated by CLM-CN, *Biogeosciences*, *9*, 509–525, doi:10.5194/bg-9-509-2012.

Krawchuk, M. A., M. A. Moritz, M.-A. Parisien, J. Van Dorn, and K. Hayhoe (2009), Global pyrogeography: The current and future distribution of wildfire, *PLoS ONE*, *4*(4), 12 p., doi:10.1371/journal.pone.0005102.

Li, F., X. D. Zeng, and S. Levis (2012), A process-based fire parameterization of intermediate complexity in a Dynamic Global Vegetation Model, *Biogeosciences*, *9*, 2761–2780, doi:10.5194/bg-9-2761-2012.

Marlon, J. R., P. J. Bartlein, C. Carcaillet, D. G. Gavin, S. P. Harrison, P. E. Higuera, F. Joos, M. J. Power, and I. C. Prentice (2008), Climate and human influences on global biomass burning over the past two millennia, *Nat. Geosci.*, *1*, 697–702, doi:10.1038/ngeo313.

Michalon, N., A. Nassif, T. Saouri, J. F. Royer, and C. A. Pontikis (1999), Contribution to the climatological study of lightning, *Geophys. Res. Lett.*, *26*(20), 3097–3100, doi:10.1029/1999GL010837.

Moss, R. H., et al. (2010), The next generation of scenarios for climate change research and assessment, *Nature*, *463*, 747–756, doi:10.1038/nature08823.

Nordeng, T. E. (1994), Extended versions of the convective parameterization scheme at ECMWF and their impact on the mean and transient activity of the model in the tropics, *Tech. Rep. 206*, ECMWF, Reading, U. K.

Pinto, O., Jr., I. R. C. A. Pinto, and K. P. Naccarato (2007), Maximum cloud-to-ground lightning flash densities observed by lightning location systems in the tropical region: A review, *Atmos. Res.*, *84*, 189–200, doi:10.1016/j.atmosres.2006.11.007.

Price, C., and D. Rind (1992), A simple lightning parameterization for calculating global lightning distribution, *J. Geophys. Res.*, *97*(D9), 9919–9933, doi:10.1029/92JD00719.

Price, C., and D. Rind (1993), What determines the cloud-to-ground lightning fraction in thunderstorms?, *Geophys. Res. Lett.*, *20*(6), 463–466, doi:10.1029/93GL00226.

Price, C., and D. Rind (1994a), Possible implications of global climate change on global lightning distributions and frequencies, *J. Geophys. Res.*, *99*(D5), 10,823–10,831, doi:10.1029/94JD00019.

Price, C., and D. Rind (1994b), The Impact of a $2xCO_2$ climate on lightning-caused fires, *J. Clim.*, *7*(10), 1484–1494, doi:10.1175/1520-0442(1994)007<1484:TIOACC>2.0.CO;2.

Price, C., and D. Rind (1994c), Modeling global lightning distributions in a general circulation model, *Mon. Weather Rev.*, *122*, 1930–1939, doi:10.1175/1520-0493(1994)122<1930:MGLDIA>2.0.CO;2.
Price, C. (2009), Thunderstorms, lightning and climate change, in *Lightning: Principles, Instruments and Applications*, edited by H. D. Betz, U. Schumann, and P. Laroche, pp. 521–535, Springer, Berlin.
Raddatz, T. J., C. H. Reick, W. Knorr, J. Kattge, E. Roeckner, R. Schnur, K.-G. Schnitzler, P. Wetzel, and J. Jungclaus (2007), Will the tropical land biosphere dominate the climate–carbon cycle feedback during the twenty-first century?, *Clim. Dyn.*, *29*, 565–574, doi:10.1007/s00382-007-0247-8.
Reick, C. H., T. Raddatz, V. Brovkin, and V. Gayler (2013), Representation of natural and anthropogenic land cover change in MPI-ESM, *J. Adv. Model. Earth Syst.*, *5*, 459–482, doi:10.1002/jame.20022.
Stevens, B., et al. (2013), Atmospheric component of the MPI-M Earth System Model: ECHAM6, *J. Adv. Model. Earth Syst.*, *5*, 146–172, doi:10.1002/jame.20015.
Stocks, B. J., et al. (2002), Large forest fires in Canada, 1959–1997, *J. Geophys. Res.*, *108*(D1), 8149, doi:10.1029/2001JD000484.
Taylor, K. E., R. J. Stouffer, and G. A. Meehl (2012), An overview of CMIP5 and the experiment design, *Bull. Am. Meteorol. Soc.*, *93*, 485–498, doi:10.1175/BAMS-D-11-00094.1.
Thonicke, K., S. Venevsky, S. Sitch, and W. Cramer (2001), The role of fire disturbances for global vegetation dynamics: Coupling fire into a Dynamic Global Vegetation Model, *Global Ecol. Biogeogr.*, *10*(6), 661–677, doi:10.1046/j.1466-822X.2001.00175.x.
Tiedtke, M. (1989), A comprehensive mass flux scheme for cumulus parameterization in large-scale models, *Mon. Weather Rev.*, *117*, 1779–1800, doi:10.1175/1520-0493(1989)117<1779:ACMFSF>2.0.CO;2.
Tost, H., P. Jöckel, and J. Lelieveld (2007), Lightning and convection parameterisations - Uncertainties in global modelling, *Atmos. Chem. Phys.*, *7*, 4553–4568, doi:10.5194/acp-7-4553-2007.
van der Werf, G. R., W. Peters, T. T. van Leeuwen, and L. Giglio (2013), What could have caused pre-industrial biomass burning emissions to exceed current rates?, *Clim. Past*, *9*, 289–306, doi:10.5194/cp-9-289-2013.
Ward, D. S., S. Kloster, N. M. Mahowald, B. M. Rogers, J. T. Randerson, and P. G. Hess (2012), The changing radiative forcing of fires: Global model estimates for past, present and future, *Atmos. Chem. Phys.*, *12*, 10,857–10,886, doi:10.5194/acp-12-10857-2012.
Williams, E. R. (2005), Lightning and climate: A review, *Atmos. Res.*, *76*, 272–287, doi:10.1016/j.atmosres.2004.11.014.